

VANGUARD: Vehicle-Anchored Ground Sample Distance Estimation for UAVs in GPS-Denied Environments

Yifei Chen^{1,3}, Xupeng Chen², Jiayin Liu¹, Feng Wang¹, and Niangang Jiao¹

Abstract—Autonomous aerial robots operating in GPS-denied or communication-degraded environments frequently lose access to camera metadata and telemetry, leaving onboard perception systems unable to recover the absolute metric scale of the scene. As LLM/VLM-based planners are increasingly adopted as high-level agents for embodied systems, their ability to reason about physical dimensions becomes safety-critical—yet our experiments show that five state-of-the-art VLMs suffer from *spatial scale hallucinations*, with median area estimation errors exceeding 50%. We propose VANGUARD, a lightweight, deterministic *Geometric Perception Skill* designed as a callable tool that any LLM-based agent can invoke to recover Ground Sample Distance (GSD) from ubiquitous environmental anchors: small vehicles detected via oriented bounding boxes, whose modal pixel length is robustly estimated through kernel density estimation and converted to GSD using a pre-calibrated reference length. The tool returns both a GSD estimate and a composite confidence score, enabling the calling agent to autonomously decide whether to trust the measurement or fall back to alternative strategies. On the DOTA v1.5 benchmark, VANGUARD achieves 6.87% median GSD error on 306 images. Integrated with SAM-based segmentation for downstream area measurement, the pipeline yields 19.7% median error on a 100-entry benchmark—with 2.6× lower category dependence and 4× fewer catastrophic failures than the best VLM baseline—demonstrating that equipping agents with deterministic geometric tools is essential for safe autonomous spatial reasoning.

I. INTRODUCTION

Micro aerial vehicles (MAVs) and unmanned aerial vehicles (UAVs) are increasingly deployed for autonomous tasks—disaster assessment, infrastructure inspection, precision agriculture, and search-and-rescue—where onboard perception must deliver metric-scale spatial understanding in real time. In GPS-denied, communication-degraded, or previously unmapped environments, these platforms routinely lose access to camera metadata and absolute telemetry, leaving monocular imagery as the sole input. Without knowing the Ground Sample Distance (GSD)—the physical size of each pixel—pixel-level measurements cannot be converted to real-world dimensions, and any downstream spatial reasoning becomes unreliable.

The robotics community has increasingly turned to vision-language models (VLMs) and large language models (LLMs) as high-level planners and agents for embodied systems [1].

However, our experiments reveal a critical failure mode: when tasked with estimating physical areas from aerial imagery alone, five state-of-the-art VLMs exhibit median errors of 38–52%, with frequent order-of-magnitude deviations. We term this failure *Spatial Scale Hallucination*—the systematic inability of VLMs to ground visual observations in metric scale without explicit geometric calibration. This poses a direct safety risk for autonomous UAV operations: a planner that misjudges a landing zone’s dimensions by 50% could attempt a catastrophic landing on an insufficiently sized surface.

We propose VANGUARD (Vehicle-ANchored Geometric Understanding And Resolution Determination)—a lightweight, deterministic *Geometric Perception Skill* and callable tool that LLM-based planners can invoke to recover absolute scale from monocular aerial imagery. Our key observation is that small vehicles are among the most ubiquitous objects in urban and suburban scenes, with physical lengths concentrated around 4–5 m worldwide. The pipeline detects vehicles via oriented bounding boxes (OBB), robustly estimates their modal pixel length through kernel density estimation (KDE), and converts it to GSD using a pre-calibrated reference length.

Our contributions are:

- A metadata-free GSD estimation method using vehicles as geometric anchors, achieving 6.87% median error on DOTA v1.5 (306 images, 67% coverage), with KDE providing 17% improvement over mean aggregation.
- Empirical evidence of *Spatial Scale Hallucination* in VLMs: a 100-entry benchmark showing that even with explicit vehicle-length hints, VLMs exhibit 2.6× higher category dependence and 4× more catastrophic failures than our deterministic pipeline.
- Integration as a *Geometric Perception Skill* for tool-augmented agents: a stateless API that accepts a monocular image and returns $(\text{GSD}_{\text{pred}}, C)$, enabling LLM/VLM planners to make safety-aware metric decisions without GPS or metadata dependencies.

II. RELATED WORK

a) *GSD and scale estimation.*: Traditional GSD determination relies on sensor specifications, flight altitude, and camera calibration [2], [3]. When metadata is unavailable, alternative approaches attempt to infer spatial scale from image content: shadow-based methods [4], monocular depth estimation [5], [6], and regression CNNs [7]. However, these methods either require supervised training with GSD labels or recover only relative depth. Wang and Wang [8] proposed

¹Aerospace Information Research Institute, Chinese Academy of Sciences, Beijing 100094, China.

²Tandon School of Engineering, New York University, New York, NY 10012, USA.

³Also with School of Electronic, Electrical and Communication Engineering, University of Chinese Academy of Sciences, Beijing 101408, China.

Corresponding author: J. Liu, liujy@mail.ie.ac.cn.

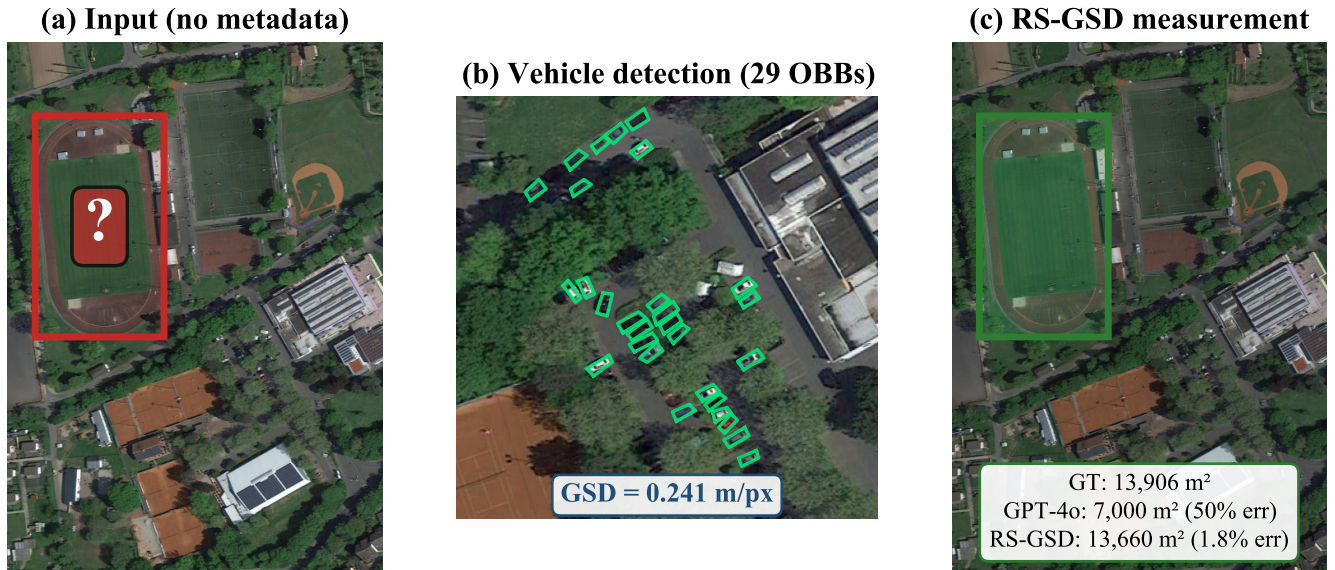


Fig. 1. Our Geometric Perception Skill in action on a DOTA v1.5 image (P2593, Ground Track Field). (a) A UAV captures an image without metadata; the target object (red box) must be measured from pixels alone. (b) Our skill detects small vehicles via oriented bounding boxes (green) and derives $GSD = 0.241$ m/px from their modal pixel length. (c) Combined with SAM segmentation, the pipeline predicts the field area within 1.8% of ground truth, whereas GPT-4o hallucinates a 50% underestimate.

a visual agentic system for scale estimation using GPT-4o-based reference object selection, but their dependence on a proprietary model limits reproducibility. We address these gaps by focusing on a single, well-characterised reference class (small vehicles) with kernel density estimation [9]–[11] for robust mode finding.

b) VLM spatial reasoning deficiencies.: Despite rapid progress in vision-language models for remote sensing [12]–[14], fundamental limitations in spatial reasoning persist. Liu et al. [15] demonstrate a large human–model gap on spatial relation tasks; Chen et al. [1] show VLMs lack 3D spatial reasoning for distance and size estimation; and Liao et al. [16] find that VLMs struggle with quantitative spatial reasoning even when provided with reference objects. These findings motivate our approach: rather than relying on VLMs for metric-scale reasoning, we provide a deterministic geometric tool that embodied agents can invoke to ground their spatial understanding.

III. METHOD

A. Overview

Given a monocular aerial image I with unknown GSD, our Geometric Perception Skill estimates GSD_{pred} (metres per pixel) using only the image content. The skill is designed as a *stateless, deterministic API*: a calling agent submits an image and receives a structured response $(GSD_{\text{pred}}, \mathcal{C})$, where $\mathcal{C} \in [0, 1]$ is a composite confidence score that the agent can use to gate downstream decisions. The pipeline consists of five stages (Fig. 2): (1) vehicle detection via OBB, (2) outlier filtering, (3) KDE mode estimation, (4) GSD computation, and (5) multi-dimensional confidence evaluation.

B. Reference Length Determination

The reference vehicle length L_{ref} is a critical parameter. Rather than selecting an arbitrary value, we derive L_{ref} statistically from the DOTA v1.5 training set, which contains 125,977 annotated “small-vehicle” instances with known GSD. For each annotation, we compute the physical vehicle length as:

$$L_i = P_i^{(\text{gt})} \times GSD_i^{(\text{gt})} \quad (1)$$

where $P_i^{(\text{gt})}$ is the OBB longer-side pixel length and $GSD_i^{(\text{gt})}$ is the ground-truth GSD of the corresponding image. We apply KDE to the distribution of $\{L_i\}$ and identify the mode:

$$L_{\text{ref}} = \arg \max_x \sum_{i=1}^N K_h(x - L_i) = 5.045 \text{ m} \quad (2)$$

This value represents the most common vehicle length in the dataset, corresponding to typical sedan-class vehicles. We note that L_{ref} is dataset-specific: the DOTA training set primarily covers Chinese urban scenes, and vehicle fleets in other regions may exhibit different modal lengths (see Limitations in Section V). The sensitivity of GSD estimation to L_{ref} is analysed in Section IV-C.

C. Vehicle Detection

We employ oriented bounding box (OBB) detection to identify small vehicles in the input image. Unlike axis-aligned detection, OBB tightly encloses each vehicle regardless of its orientation, providing accurate pixel-length measurements.

The detector outputs a set of N detections $\{(P_i, C_i)\}_{i=1}^N$, where P_i is the longer side of the OBB in pixels and $C_i \in$

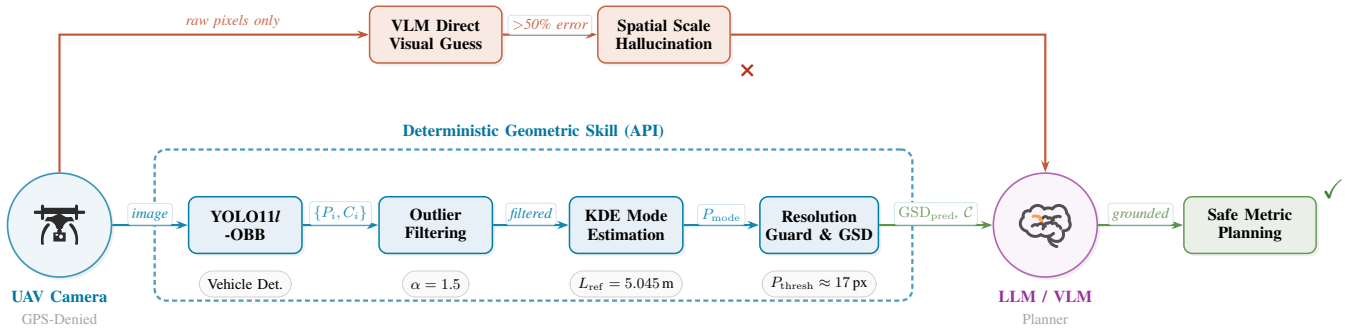


Fig. 2. System architecture as an Embodied Agent Perception Loop. **Left**: a UAV operating in a GPS-denied environment captures monocular imagery. **Centre** (dashed box): our Deterministic Geometric Skill processes the image through YOLO-OBb detection, outlier filtering, KDE mode estimation, and a resolution guard to produce a calibrated GSD with confidence score. **Right**: the LLM/VLM Planner can either rely on direct visual estimation (red path), suffering from Spatial Scale Hallucination (>50% error), or invoke our Geometric Skill (green path) for safe metric planning.

$[0, 1]$ is the detection confidence score. Detections with $C_i < 0.1$ are discarded.

For large remote sensing images (e.g., 4000×4000 pixels), we apply a tiling strategy: the image is divided into overlapping tiles, detection is run on each tile, and results are merged with non-maximum suppression to handle tile-boundary duplicates.

D. Outlier Filtering

Vehicle detections may include false positives (e.g., rooftop structures, road markings) or genuine vehicles of atypical size (buses, trucks). We apply a simple median-based outlier filter:

$$\text{Keep detection } i \text{ iff } P_i \leq \alpha \cdot \text{median}(\{P_j\}_{j=1}^{N'}) \quad (3)$$

where $\alpha = 1.5$ is the outlier factor. This preserves the majority of small vehicles while removing large outliers that would distort the pixel-length distribution. The sensitivity to α is examined in Section IV-C.

E. KDE Mode Estimation

Given the filtered pixel lengths $\{P_i\}_{i=1}^{N'}$, we estimate the modal pixel length P_{mode} using kernel density estimation. The density function is:

$$\hat{f}(x) = \frac{1}{N'} \sum_{i=1}^{N'} K_h(x - P_i) \quad (4)$$

where $K_h(\cdot)$ is a Gaussian kernel with bandwidth h selected via Scott's rule. The modal pixel length is:

$$P_{\text{mode}} = \arg \max_x \hat{f}(x) \quad (5)$$

Unlike simple summary statistics (mean, median), KDE captures the full distributional shape and identifies the true mode, making it robust to skewed distributions caused by false positives or atypical vehicles. A weighted variant using detection confidence C_i as KDE weights is evaluated in the ablation study (Section IV-C) but provides no measurable improvement over unweighted KDE.

When fewer than 5 detections survive filtering ($N' < 5$), KDE is unreliable due to insufficient samples. In this regime, we fall back to the simple median of pixel lengths.

Finally, GSD is computed as:

$$\text{GSD}_{\text{pred}} = \frac{L_{\text{ref}}}{P_{\text{mode}}} \quad (6)$$

F. Confidence Evaluation and Safety Fallback

Each GSD prediction is accompanied by a composite confidence score $\mathcal{C} \in [0, 1]$ aggregating four dimensions via a weighted sum: (1) sample sufficiency ($w = 0.35$), penalising few detections; (2) distribution concentration ($w = 0.35$), rewarding low coefficient of variation; (3) detection quality ($w = 0.20$), reflecting median YOLO confidence; and (4) anomaly detection ($w = 0.10$), flagging physically implausible pixel lengths.

a) *Autonomous safety fallback.*: The composite score is blind to a critical physical limitation: at coarse resolution ($\text{GSD} \gtrsim 0.3$ m/px), vehicles are detected with consistent but systematically compressed pixel lengths, causing the score to remain high despite large GSD errors. For safe autonomous operation, we augment \mathcal{C} with a hard resolution guard:

$$\mathcal{C} = \begin{cases} \mathcal{C}_{\text{raw}} & \text{if } P_{\text{mode}} \geq P_{\text{thresh}} \\ \min(\mathcal{C}_{\text{raw}}, 0.3) & \text{if } P_{\text{mode}} < P_{\text{thresh}} \end{cases} \quad (7)$$

where $P_{\text{thresh}} = L_{\text{ref}}/\text{GSD}_{\text{max}}$ with $\text{GSD}_{\text{max}} = 0.3$ m/px, yielding $P_{\text{thresh}} \approx 17$ pixels. This threshold adapts automatically when L_{ref} is recalibrated for a different region. A UAV planner receiving $\mathcal{C} < 0.5$ should autonomously fall back to alternative localisation strategies (e.g., altitude hold, visual odometry) rather than trusting the GSD estimate—this confidence-gated design allows the calling agent to maintain a safe decision loop without human intervention.

IV. EXPERIMENTS

A. Dataset and Setup

We evaluate on the DOTA v1.5 dataset [17], [18]. Although primarily comprising high-resolution satellite imagery, DOTA serves as a standard, rigorous proxy for

TABLE I

GSD ESTIMATION RESULTS ON DOTA v1.5 VALIDATION SET (458 IMAGES TOTAL). THE GT BASELINE USES GROUND-TRUTH ANNOTATIONS (269 IMAGES). THE “INTERSECTION” ROWS RESTRICT BOTH E2E AND GT TO THE 267 IMAGES COVERED BY BOTH EVALUATIONS, ENABLING A LIKE-FOR-LIKE COMPARISON.

Detector	Evaluated	Median Err	Mean Err	<10%	<20%
YOLOv8m-OBb (v1)	310	7.17%	14.88%	63.2%	80.0%
YOLOv8l-OBb (v2)	310	6.87%	13.44%	65.2%	82.3%
YOLO11l-OBb (v3)	306	6.87%	12.89%	66.0%	83.3%
GT Baseline (all)	269	6.88%	8.54%	67.7%	92.6%
YOLO11l-OBb (v3, intersection)	267	6.22%	9.41%	71.9%	89.5%
GT Baseline (intersection)	267	6.88%	8.56%	67.4%	92.5%

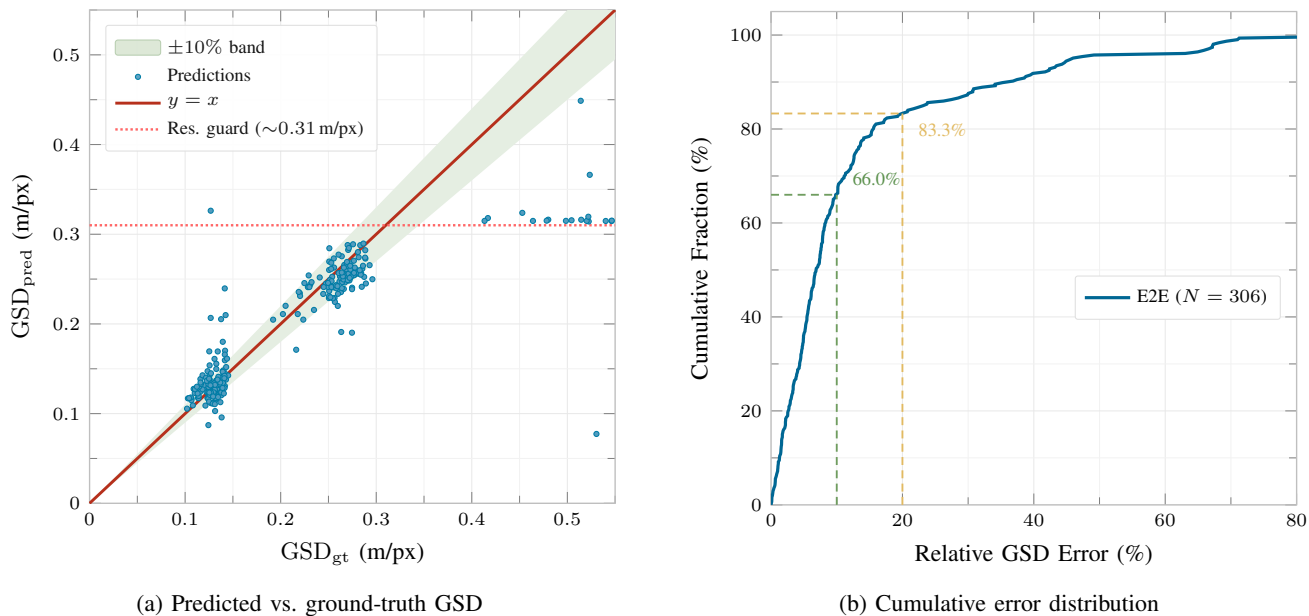


Fig. 3. End-to-end GSD estimation results (YOLO11l-OBb, 306 images). (a) Predicted vs. ground-truth GSD for images with GSD < 0.55 m/px (271 of 306 images). The shaded band denotes $\pm 10\%$ error; the horizontal dotted line at $\text{GSD}_{\text{pred}} \approx 0.31$ m/px marks the resolution guard limit ($P_{\text{mode}} \approx 16$ px), beyond which predictions saturate. (b) Cumulative error distribution: 66.0% of images achieve < 10% error (green dashed) and 83.3% achieve < 20% error (amber dashed). The long tail corresponds primarily to low-resolution images (GSD > 0.3 m/px).

TABLE II

AREA ESTIMATION ON RS-GSD BENCHMARK v5.0 (100 ENTRIES, 8 CATEGORIES). UPPER: ZERO-SHOT VLMS. MIDDLE: VLMS WITH VEHICLE-LENGTH HINT. LOWER: OUR PIPELINE.

Model	Med. Err.	Mean Err.	<10%	<25%	<50%	<100%
<i>Zero-shot (no scale information):</i>						
Qwen2.5-VL-72B	38.3%	84.5%	19%	35%	61%	84%
Claude Opus 4.6	47.2%	72.9%	24%	35%	55%	73%
Qwen-VL-Max	50.3%	97.1%	13%	27%	49%	75%
Qwen-VL-Plus	51.3%	190.3%	22%	33%	49%	68%
GPT-4o	51.9%	69.4%	17%	34%	48%	93%
<i>With vehicle-length hint (“cars ≈ 5 m”):</i>						
Claude Opus 4.6 + hint [†]	17.1%	41.5%	36%	59%	73%	88%
GPT-4o + hint	35.9%	55.2%	15%	36%	59%	85%
Qwen2.5-VL-72B + hint	38.1%	100.4%	10%	30%	59%	83%
Qwen-VL-Max + hint	46.5%	99.9%	13%	30%	53%	80%
Qwen-VL-Plus + hint	58.0%	236.2%	12%	28%	44%	70%
RS-GSD (ours)	19.7%	29.2%	30%	59%	80%	97%

[†]Claude Opus 4.6 operates as an *agent* with programmatic image analysis tools, unlike other VLMS which perform pure visual estimation.

high-altitude UAV nadir views due to its equivalent perspective and precise GSD metadata. The dataset contains

high-resolution aerial images with oriented bounding box annotations for 16 object categories. We use the “small-

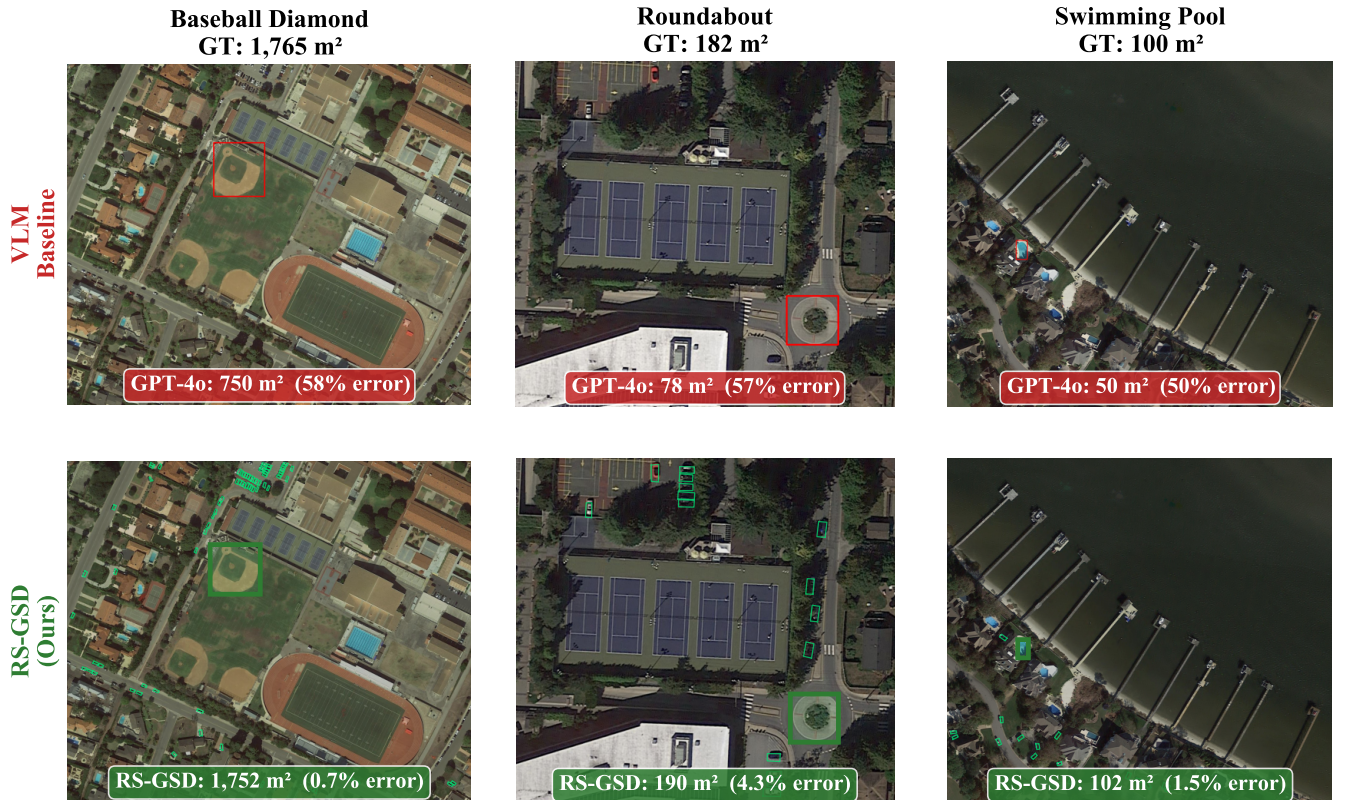


Fig. 4. Qualitative comparison on three benchmark entries. **Top:** annotated input with GPT-4o predictions (red). **Bottom:** RS-GSD pipeline with vehicle OBBs (green) and SAM segmentation overlay. Our geometric approach achieves 0.7–4.3% error vs. GPT-4o’s 50–58% error, illustrating the spatial scale hallucination phenomenon.

vehicle” category for training the vehicle detector. Critically, DOTA images include GSD metadata, enabling quantitative evaluation of our GSD predictions.

The dataset comprises 1,411 training images and 458 validation images. For detector training, we split the training set into an 85% Training Subset and a 15% Dev Set for hyperparameter tuning. The full 458-image validation set serves as our test set. Of these, 8 images lack GSD metadata and are excluded, leaving 450 evaluable images.

We evaluate GSD estimation accuracy using the relative error:

$$\epsilon_{\text{rel}} = \frac{|\text{GSD}_{\text{pred}} - \text{GSD}_{\text{gt}}|}{\text{GSD}_{\text{gt}}} \quad (8)$$

We report median and mean relative error, as well as the proportion of images with $\epsilon_{\text{rel}} < 10\%$ and $\epsilon_{\text{rel}} < 20\%$.

B. Vehicle Detection and GSD Evaluation

We train YOLO11i-OBB [19] on the DOTA v1.5 Training Subset for oriented vehicle detection, achieving mAP50 = 0.660 on the Dev Set. Using ground-truth annotations as an upper bound, the statistical pipeline achieves 6.88% median GSD error on 269 images—the irreducible error from vehicle length variability.

End-to-end, replacing GT annotations with YOLO detections, the pipeline achieves 6.87% median error on 306 images (67% coverage). On the 267-image intersection of

E2E and GT evaluation sets, E2E achieves 6.22% median error vs. the GT baseline’s 6.88%, confirming that KDE mode estimation effectively absorbs detection noise. The pipeline produces no estimate for 152 images (33%) lacking detectable vehicles; these receive $\mathcal{C} = 0$.

The gap between E2E and GT is larger for mean error (12.89% vs. 8.54%) due to images with < 5 detections where the fallback median estimator is less accurate.

C. Ablation and Sensitivity Analysis

Table III consolidates the key ablation findings.

a) *Key findings.*: KDE mode estimation outperforms mean aggregation by 17% relative improvement (6.87% vs. 8.27% E2E median error), as KDE captures the distributional shape and is robust to outliers. The reference length L_{ref} is the most sensitive parameter: a ± 0.5 m deviation roughly doubles the median error, validating data-driven calibration. Performance scales with vehicle count (≥ 20 vehicles: 6.12%; < 5 : 13.47%) and degrades sharply at coarse resolution (> 0.7 m/px: 67%), confirming the method’s operating envelope of sub-metre urban imagery. The confidence score ($r = -0.354$ with error) provides coarse quality gating; the resolution guard correctly flags 35 of 51 high-error images.

TABLE III
 ABLATION AND SENSITIVITY ANALYSIS. ALL RESULTS USE GT
 ANNOTATIONS (269 IMAGES) UNLESS NOTED. “E2E” USES
 YOLO11I-ORB DETECTIONS (306 IMAGES).

Factor	Setting	Med. Err	<20%
<i>Aggregation method (E2E):</i>			
	KDE (ours)	6.87%	83.3%
	Median	7.31%	84.0%
	Mean	8.27%	83.7%
<i>Reference length L_{ref}:</i>			
	4.5 m	10.59%	80.3%
	5.045 m (ours)	6.88%	92.6%
	5.5 m	10.71%	79.9%
<i>Outlier factor α:</i>			
	1.0	7.27%	87.7%
	1.5 (ours)	6.88%	92.6%
	None	6.74%	92.6%
<i>Vehicle count (E2E):</i>			
	$N \geq 20$	6.12%	—
	$N < 5$	13.47%	—
<i>GSD range (E2E):</i>			
	< 0.3 m/px	6.10%	—
	> 0.7 m/px	67.19%	—

D. Spatial Scale Hallucination: RS-GSD vs. VLMs

To quantify VLM spatial hallucinations, we benchmark area estimation: $A = N_{\text{px}} \times \text{GSD}^2$. The *RS-GSD Benchmark v5.0* (100 entries, 64 images, 8 categories from iSAID [20] \cap DOTA v1.5) deliberately oversamples irregular objects (swimming pools, roundabouts) to stress-test memorised-size priors. We evaluate five VLMs [21]–[24] in zero-shot and vehicle-length-hinted settings; our pipeline uses YOLO-ORB + SAM [25] segmentation.

a) *Results.*: Table II reveals severe spatial hallucinations: all zero-shot VLMs cluster at 38–52% median error. With a vehicle-length hint (“cars \approx 5 m”), only Claude (17.1%, using programmatic tools[†]) and GPT-4o (35.9%) improve meaningfully; Qwen models show negligible or negative change. Our RS-GSD pipeline achieves 19.7% median error with $2.6\times$ lower category dependence (polarisation ratio $1.9\times$ vs. $5.0\times$) and $4\times$ fewer catastrophic failures ($<100\%$: 97% vs. 88%). The tight median-mean gap of our pipeline (19.7% vs. 29.2%) versus VLMs (e.g., 38.3% vs. 84.5% for Qwen2.5-VL-72B) confirms that geometric measurement is fundamentally more reliable than visual estimation.

V. DISCUSSION

a) *Deterministic vs. learned spatial reasoning.*: Our experiments demonstrate a fundamental gap between VLM-based spatial reasoning and deterministic geometric measurement. KDE mode estimation outperforms mean aggregation by 17%, and even with explicit vehicle-length hints, most VLMs cannot translate this prior into accurate area estimates—confirming the spatial scale hallucination phenomenon [1], [15], [16]. This finding supports the emerging *tool-augmented agent* paradigm: rather than expecting end-to-end models to master every perceptual modality, we equip

LLM/VLM planners with specialised, deterministic tools for tasks that demand metric precision. VANGUARD instantiates this paradigm for spatial scale: the planner delegates GSD estimation to our geometric skill and receives a confidence-gated result, preserving the agent’s high-level reasoning capability while grounding its spatial understanding in physics.

b) *Limitations.*: The method requires small vehicles in the scene (absent in 33% of DOTA images) and sub-metre resolution ($\text{GSD} \lesssim 0.3$ m/px). The reference length $L_{\text{ref}} = 5.045$ m is calibrated for Chinese urban fleets; deployment in other regions requires recalibration (± 0.5 m deviation roughly doubles error). Oblique or off-nadir imagery would introduce perspective distortion not modelled by our pipeline. Extending to multiple reference object classes (e.g., road lane widths, shipping containers) could improve coverage.

VI. CONCLUSION

We have presented VANGUARD, a lightweight, deterministic Geometric Perception Skill that equips tool-augmented embodied agents with the ability to recover absolute metric scale from monocular aerial imagery without GPS or camera metadata. By detecting ubiquitous small vehicles and estimating their modal pixel length via KDE, our method achieves 6.87% median GSD error on DOTA v1.5 (306 images). Integrated with SAM segmentation for area measurement, the pipeline yields 19.7% median error on a 100-entry benchmark—with $2.6\times$ lower category dependence and 97% of predictions within 100% error—while five state-of-the-art VLMs exhibit severe spatial scale hallucinations (38–52% median error zero-shot). These results demonstrate that the tool-augmented agent paradigm—where LLM planners delegate metric-critical perception to deterministic geometric skills—is essential for safe autonomous spatial reasoning. Future work includes extending to multiple reference object classes, validating on diverse geographic regions, and integrating VANGUARD into closed-loop UAV planning systems as a standard perception tool alongside depth estimation and obstacle detection.

REFERENCES

- [1] B. Chen, Z. Xu, S. Kirmani, B. Ichter, D. Sadigh, L. Guibas, and F. Xia, “SpatialVLM: Endowing vision-language models with spatial reasoning capabilities,” in *Proceedings of the IEEE/CVF Conference on Computer Vision and Pattern Recognition (CVPR)*, 2024, pp. 14 455–14 465.
- [2] P. R. Wolf, B. A. DeWitt, and B. E. Wilkinson, *Elements of Photogrammetry with Applications in GIS*, 4th ed. New York: McGraw-Hill Education, 2014.
- [3] T. Toutin, “Review article: Geometric processing of remote sensing images: models, algorithms and methods,” *International Journal of Remote Sensing*, vol. 25, no. 10, pp. 1893–1924, 2004.
- [4] G. Liasis and S. Stavrou, “Satellite images analysis for shadow detection and building height estimation,” *ISPRS Journal of Photogrammetry and Remote Sensing*, vol. 119, pp. 437–450, 2016.
- [5] R. Ranfil, K. Lasinger, D. Hafner, K. Schindler, and V. Koltun, “Towards robust monocular depth estimation: Mixing datasets for zero-shot cross-dataset transfer,” *IEEE Transactions on Pattern Analysis and Machine Intelligence*, vol. 44, no. 3, pp. 1623–1637, 2022.
- [6] S. F. Bhat, R. Birkl, D. Wofk, P. Wonka, and M. Müller, “Zoedepth: Zero-shot transfer by combining relative and metric depth,” *arXiv preprint arXiv:2302.12288*, 2023.

- [7] J. H. Lee and S. Sull, "Regression tree CNN for estimation of ground sampling distance based on floating-point representation," *Remote Sensing*, vol. 11, no. 19, p. 2276, 2019.
- [8] Y. Wang and C. Wang, "Visual agentic system for spatial metric query answering in remote sensing images," in *Eurographics 2025*. The Eurographics Association, 2025.
- [9] M. Rosenblatt, "Remarks on some nonparametric estimates of a density function," *The Annals of Mathematical Statistics*, vol. 27, no. 3, pp. 832–837, 1956.
- [10] E. Parzen, "On estimation of a probability density function and mode," *The Annals of Mathematical Statistics*, vol. 33, no. 3, pp. 1065–1076, 1962.
- [11] B. W. Silverman, *Density Estimation for Statistics and Data Analysis*. London: Chapman and Hall, 1986.
- [12] K. Kuckreja, M. S. Danish, M. Naseer, A. Das, S. Khan, and F. S. Khan, "GeoChat: Grounded large vision-language model for remote sensing," in *Proceedings of the IEEE/CVF Conference on Computer Vision and Pattern Recognition (CVPR)*, 2024, pp. 27 831–27 841.
- [13] X. Li, C. Wen, Y. Hu, Z. Yuan, and X. X. Zhu, "Vision-language models in remote sensing: Current progress and future trends," *IEEE Geoscience and Remote Sensing Magazine*, vol. 12, no. 2, pp. 56–86, 2024.
- [14] F. Liu, D. Chen, Z. Guan, X. Zhou, J. Zhu, Q. Ye, L. Fu, and J. Zhou, "RemoteCLIP: A vision language foundation model for remote sensing," *IEEE Transactions on Geoscience and Remote Sensing*, vol. 62, pp. 1–13, 2024.
- [15] F. Liu, G. Emerson, and N. Collier, "Visual spatial reasoning," *Transactions of the Association for Computational Linguistics*, vol. 11, pp. 635–651, 2023.
- [16] Y.-H. Liao, R. Mahmood, S. Fidler, and D. Acuna, "Reasoning paths with reference objects elicit quantitative spatial reasoning in large vision-language models," in *Proceedings of the 2024 Conference on Empirical Methods in Natural Language Processing*. Association for Computational Linguistics, 2024, pp. 17 028–17 047.
- [17] G.-S. Xia, X. Bai, J. Ding, Z. Zhu, S. Belongie, J. Luo, M. Datcu, M. Pelillo, and L. Zhang, "DOTA: A large-scale dataset for object detection in aerial images," in *Proceedings of the IEEE/CVF Conference on Computer Vision and Pattern Recognition (CVPR)*, 2018, pp. 3974–3983.
- [18] J. Ding, N. Xue, G.-S. Xia, X. Bai, W. Yang, M. Y. Yang, S. Belongie, J. Luo, M. Datcu, M. Pelillo, and L. Zhang, "Object detection in aerial images: A large-scale benchmark and challenges," *IEEE Transactions on Pattern Analysis and Machine Intelligence*, vol. 44, no. 11, pp. 7778–7796, 2022.
- [19] G. Jocher and J. Qiu, "Ultralytics YOLO11," <https://github.com/ultralytics/ultralytics>, 2024, version 11.0.0.
- [20] S. Waqas Zamir, A. Arora, A. Gupta, S. Khan, G. Sun, F. S. Shah, F. Zhu, L. Shao, G.-S. Xia, and X. Bai, "iSAID: A large-scale dataset for instance segmentation in aerial images," in *Proceedings of the IEEE/CVF Conference on Computer Vision and Pattern Recognition Workshops (CVPRW)*, 2019, pp. 28–37.
- [21] S. Bai, K. Chen, X. Liu, J. Wang, W. Ge, S. Song, K. Dang, P. Wang, S. Wang, J. Tang *et al.*, "Qwen2.5-VL technical report," *arXiv preprint arXiv:2502.13923*, 2025.
- [22] Anthropic, "Claude: Model overview," <https://docs.anthropic.com/en/docs/about-claude/models>, 2025, claude Opus 4.6 (model ID: claude-opus-4-6), accessed February 2026.
- [23] P. Wang, S. Bai, S. Tan, S. Wang, Z. Fan, J. Bai, K. Chen, X. Liu, J. Wang, W. Ge *et al.*, "Qwen2-VL: Enhancing vision-language model's perception of the world at any resolution," *arXiv preprint arXiv:2409.12191*, 2024.
- [24] OpenAI, "GPT-4o system card," *arXiv preprint arXiv:2410.21276*, 2024.
- [25] A. Kirillov, E. Mintun, N. Ravi, H. Mao, C. Rolland, L. Gustafson, T. Xiao, S. Whitehead, A. C. Berg, W.-Y. Lo *et al.*, "Segment anything," in *Proceedings of the IEEE/CVF International Conference on Computer Vision (ICCV)*, 2023, pp. 4015–4026.